Investigating The Dependence of the 3-Phase Cage Motor Starting Torque on The Rotor Bar Taper Angle

OMOGBAI NELSON OYAKHILOMEN[1], OBUTE KINGSLEY CHIBUEZE[2]
[1,2]*Electrical Engineering Department, Nnamdi Azikiwe University, Awka, Anambra State, Nigeria.*

ABSTRACT - The paper unveils the relative influence of design changes in the angle of taper of the 3ph squirrel cage induction motor rotor bar cross section, on the starting torque of the machine. The influence of the bar cross sectional area (CSA), top width and the radial depth of the bar section, as established design variables, were also investigated so as to know where the degree of influence of the taper angle falls in comparison, as far as the starting torque is concerned. The machines were investigated in their steady state operating mode using the equivalent circuit method. The machine learning capabilities of the Least Square Support Vector Machine (LSSVM) was deployed to extract by prediction, information about the likely dependencies between the randomized block of the geometric variables and the Starting torque, and the captured information was stored using the Root Mean Square Error (RMSE) of predictions. The validated results show that the leakage reactance and resistance of the rotor tends to be significantly sensitive to a design change in the taper angle of the transverse section of the rotor bar.

Indexed Terms - Taper angle, Starting torque, Rotor leakage reactance, Rotor resistance, RMSE, Machine learning. LSSVM,

I. INTRODUCTION

The squirrel-cage induction motor (SCIM) happens to be the most adopted electrical machine for electrical drives [1]. Studies have shown that to improve the performance of a SCIM, several design variables may have to be modified; one of such adjustments being the optimization of the stator and rotor geometries [2]. The rotor slot geometry which can be considered as an independent design parameter, is the most influential factor in defining the torque-speed characteristic of the SCIM, especially when mains fed [2],[3].

The authors in [15] highlighted that the rotor slots are always shaped such that they narrow or enlarge along the radial height to take advantage of the required skin effect during starting. Further, the rotor slot geometries which tend to reduce the width of the bar in the direction of the slot opening, produce a better starting torque and a shorter starting time, since the current tends to flow in the upper part of the rotor bar [16]. In [11], it was also buttressed that a fat tooth discourages saturation in the main flux path by carrying more flux down the tooth lengths and across the air gap, but teeth that are too fat necessitate slots that are too narrow and result in slot leakage flux that is too high. Leakage flux is increased in narrow teeth because some of the flux is forced to seek alternate paths other than down the lengths of the teeth [11].

As the slot leakage flux in the rotor crowds towards the shaft direction of the bar, leaving the top with a lower reactance; the bar current will crowd towards a smaller portion of the cross section at the top of the bar to face a low inductance path and a high frequency-dependent equivalent ac resistance results – a condition that is needed for a good starting torque (T_{st}) [8],[17]. The deep bar effect that prevails during high slip condition tends to render a good part of the geometric range of the bar depth and CSA unavailable to carry the starting current (I_{st}); because the entire rotor current is forced to crowd at the top section of the rotor bar.

Studies like, [1], [2] and [6]; also appear to establish that T_{st} depends more on the geometry of the portion of the bar section closest to the airgap than it depends on any other bar configurations. Under the constant area constraint, the highest value of T_{st} from all the variants of the rotor bar studied by the authors happens to be found in the instance of the largest ratio of the heights of the upper (narrower) portion to the heights of the lower portion of the stepped bar.

A rotor slot shape that is deep and narrow, allows considerable magnetic flux to cross the slot. In [8], the author opined that when the slot width increases, the overall slot permeance decreases as a result. This decreases the slot leakage flux and thus the leakage reactance of the stator or rotor. In [9], the authors emphasized that as the height of the rotor slot increases, permeance factor and slot inductance increases. The torque developed is inversely proportional to rotor inductance [13]. By varying the slot width and height, the slot permeance factor changes [9].

The researcher or designer in practice shall by the outcome of this study be able to ascertain critical variables of the bar section to focus on for the finetuning of the starting (T_{st}) torque, and together with other essential stator and rotor variables, may become more guided towards the optimal infeed to the computer algorithms/programs; for easier, more efficient and precise realization of distinct machine designs of target performance.

II. MATERIALS AND METHODS

First, two 3ph SCIMs of ratings 100 HP (M1) and 75HP (M2) were run in MATLAB for the purpose of conducting this study and their specifications are given in Table 1

Second, all variables of machine M1 were kept constant while altering only the geometric parameters of the rotor bar cross section such as the bar cross sectional area (A), top width (W), the radial depth (D), and the angle of taper (T); all varied at the same time. The starting torque responses were recorded against the corresponding varied geometric parameters at each instance of variation, as far as the constraints were not violated and as far as the machine performance indices remain within acceptable limits.

Third, using the tunelssvm, trainlssvm and simlssvm commands from [14], the Least Square Support Vector Machine (LSSVM) was tuned and trained on one part of the collated data (namely, the training dataset) and deployed on the second part (namely, the various blocks of test dataset); to unravel by predicting with the randomized trial procedure, the levels of the underlying dependence that the starting torque may likely have on the various randomized blocks of the bar geometric parameters. The randomized blocks were investigated this way using the RMSE of the separate predictions as the metric of comparing the results. The following randomization was applied to the geometric parameter blocks of the rotor bar section:

Lone blocks – A (rotor bar CSA), W (rotor bar top width), D (bar radial depth), and T (angle of taper).
Duo blocks – WT, DW. WA, DT, DA, TA.
Triad blocks – WDT, WTA, WDA, DTA,
Quad blocks –WDTA,

The most accurate results were then ranked in Table 2. All of the foregoing procedure were repeated with machine M2 which houses rotor bars of completely different design, so as to verify if the observed results are specific to a given machine design or generic within the family of the three-phase SCIMs. The block with the most accurate prediction (least RMSE) for each machine was noted and thoroughly analyzed with the relevant portions of literature, so as to properly situate, prune and finetune the Machine Learning (ML) result.

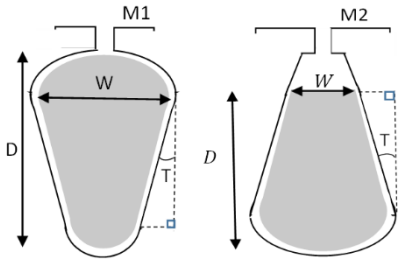

Fig 1: Rotor bar configurations

Table 1: Machine specification

Paramaters	M1	M2
Number of poles (p)	8	6
Number of rotor slots (Sr)	55	55
Number of stator slots (Ss)	72	72
Full load efficiency (EffR) %	91.12268	91.01281
Full load current (I1R) Amps	137.6654	104.0402
Full load power factor (PFR)	0.858292	0.851315
Full load speed (nmR) rpm	738.5339	988.1062
Full load torque (TTdR) N.m	972.3505	545.2107
Starting Torque (Tst) N.m	1211.621	1033.852
Maximum Torque (Tmax) N.m	3368.963	2406.64
X1 (ohms)	0.119191	0.109422
X2pr (ohms)	0.132793	0.136917
Xm (ohms)	3.939174	4.741772
R1 (ohms)	0.035604	0.055372
R2pr (ohms)	0.042764	0.049827
Rc (ohms)	110.508	157.5086

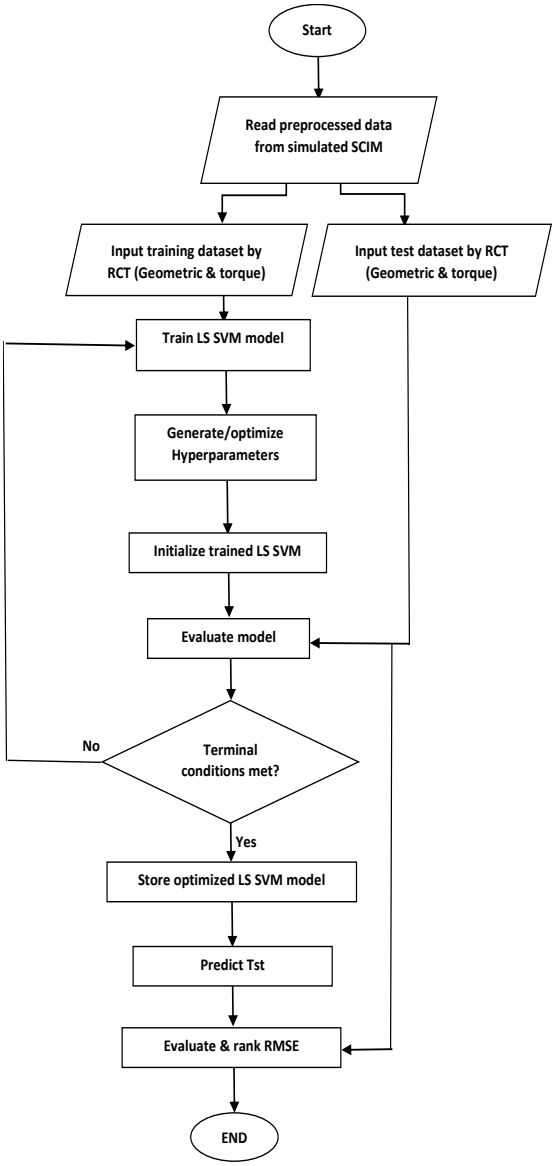

Fig 1,2: Machine learning flowchart

III. RESULTS AND DISCUSSION

Table 2: Results from machine learning (ML)

(M1) Geometric Blocks	(Tst) RMSE		(M2) Geometric Blocks	(Tst) RMSE
WT	5.86E-09		DT	4.2E-09
T	6.13E-09		T	4.32E-09
DT	6.51E-09		WT	5.3E-09

Table 2 shows that for both machines M1 and M2, the ML tends to respectively put forward the geometric blocks WT and DT as priority, as far as the influence of bar geometry on the starting torque is concerned. Also, among the investigated lone blocks of A, W, D and T; the T_{st} turns out to be most sensitive to design changes in the angle of taper – block T. According to [4];

$$T_{st} = \frac{3p}{2}\frac{R_R}{\omega_e}\left(\frac{U_S}{X_{Ye}}\right)^2 \quad (1.1)$$

In "(1.1)", U_S is the peak value of the phase voltages, R_R is the rotor resistance, p is the number of pole pairs, ω_e is the frequency of stator voltages, and currents, and reactance X_{Ye} represent the equivalent leakage reactance of the rotor and stator windings of the equivalent two-phase rotor winding that represent the rotor cage and are referred to the stator side.

A. Rotor of Machine M1

From design perspective, studies have shown that at high slip, R_R is the main means of influencing I_{ST} [5]. From basic knowledge of electric current flow, we know that the impedance (or resistance) of a conductor under a constant potential difference, is inversely proportional to the current flow through it. i.e.,

$$I_{ST} \propto 1/R_R \quad (1.2)$$

From Nene in [18], the AC resistance R_R was given as:

$$R_R \approx \frac{\rho L}{A}\left(\frac{D}{\partial}\right) \quad (1.3)$$

Where, ρ and L are respectively the resistivity and axial length of the rotor bar.

A and D are the investigated parameters of area and depth of bar respectively.

∂ is the skin depth – the depth of penetration of the AC current in the rotor bar which inversely varies with frequency. Since the bar top width W α A, then W α

$$1/R_R \propto I_{ST} \quad (1.4)$$

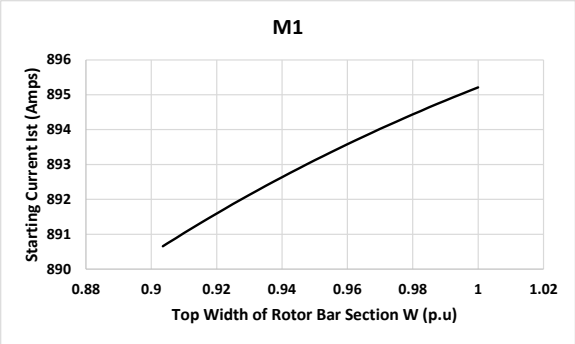

Fig 2a: Influence of change in bar top width on starting current (Machine M1).

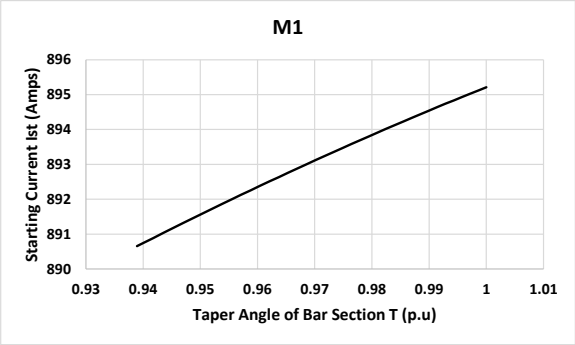

Fig 2b: Influence of change in bar taper angle on starting current (Machine M1).

A closer examination of Fig 2a shows that I_{ST} appears to increase with W, and this tends to agree with "(1.4)" because a reduction in W invariably means a drop in the area of the portion of the cross section at the top, that is, a rise in rotor resistance and therefore a drop in I_{ST} together with a rise in T_{ST} (see Fig 3) according to "(1.1)".

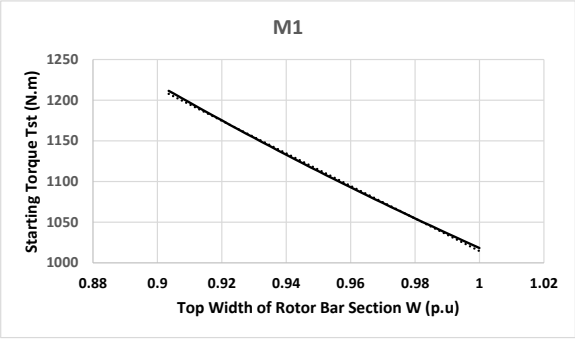

Fig 3a: Influence of change in bar top width on starting torque (Machine M1).

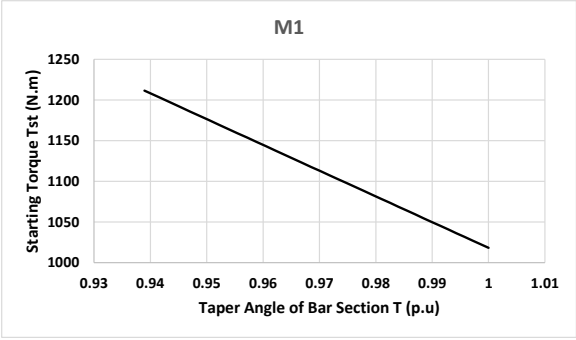

Fig 3b: Influence of change in bar taper angle on starting torque (Machine M1).

On the other hand, to observe that I_{ST} also tends to increase with T, is equally in order because due to the method of simulation, the taper angle was increasing as a result of a constant bottom width and a greater rate of increase in W relative to D, which tends to increase the cross-sectional area A at the top (some R_2 drop, as in Fig 4) relative to the slot bottom, thus there is likely to be more cross slot flux and more leakage inductance at the bottom relative to the bar top and hence more current density at the top.

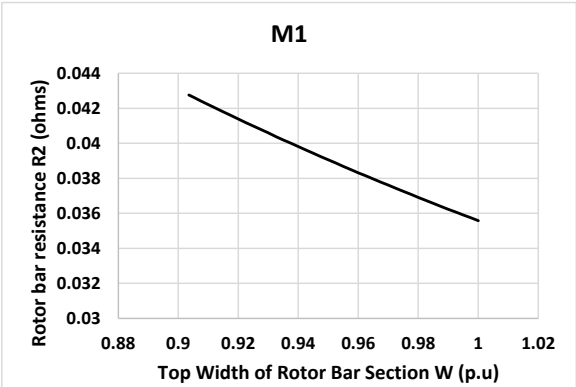

Fig 4a: Influence of change in bar top width on rotor resistance (Machine M1).

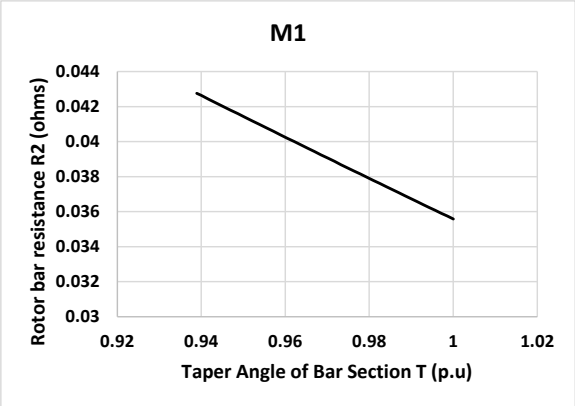

Fig 4b: Influence of change in bar taper angle on rotor resistance (Machine M1).

This development according to [11] and [19]; may cause the flow of more current to meet the useful torque demand. Equation (1,1) shows that a rise in the total rotor leakage reactance diminishes T_{ST}, hence figure 3 appears valid for both W and T.

Further, Fig 5 shows that the total rotor leakage reactance X_2 tends to increase with both W and T. Equations (1,5) through (1.7) reveals that this appears to be true for T. But from basic electromagnetic theory e.g. in [13], we know that X_2 increases with the leakage flux level ϕ_l, which in turn relates inversely to the reluctance of the cross slot leakage flux path R_l, which in turn is proportional to the length of the leakage flux path L_l. That is:

$$X_2 \text{ α } \phi_l = \frac{MMF}{R_l} \qquad (1.5)$$

Also,

$$R_l \text{ α } L_l \text{ α } 1/(slot\ narrowness) \text{ α } 1/T \qquad (1.6)$$

Therefore, the X_2 is likely to rise with the angle of slot taper T i.e., X_2 α T (1.7)

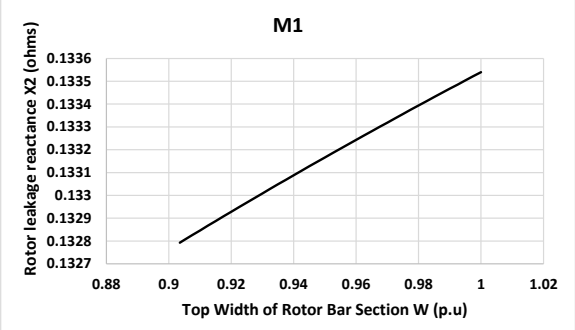

Fig 5a: Influence of change in bar top width on rotor leakage reactance (Machine M1).

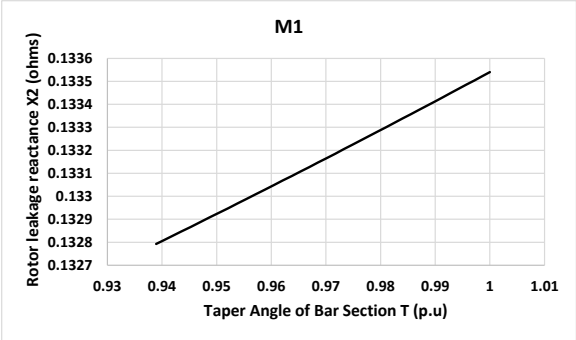

Fig 5b: Influence of change in bar taper angle on rotor leakage reactance (Machine M1).

On the other hand, an increase in W is unlikely to cause a rise in slot leakage flux except it results in the increase in slot taper. However, W could be increased to the limit where the bar area at the top becomes too large (from low R_R) and a high I_{st} brings about leakage flux path saturation [8]. Reference [12] gives support to the inverse X_2/T_{st} relation for M1 because a rise in X_2 connotes a drop in the rotor circuit power factor which means a decrease in torque production (T_{em}) according to the relation in "(1.8)".

$$T_{em} \text{ α } \phi I_2 \,.\, (rotor\ power\ factor) \qquad (1.8)$$

We may therefore deduce from the foregoing that for the rotor configuration of M1 with or without a sufficient bar depth to promote skin effect, the R_R (or R_2) appears to be governed by W, while T seems to be mainly in charge of X_2. This tends to highlight the significance of both of the design variables of block W and T in influencing the T_{st}.

B. Rotor of Machine M2

The rotor slot geometries which tend to reduce the width of the bar in the direction of the slot opening (as in M2), produce a better starting torque and a shorter starting time, since the current tends to flow in the upper part of the rotor bar [16]. So, the current crowding at the bar top due to skin effect is constrained to flow through the narrowest portion of the cross section – this means a relatively curtailed I_{st}, higher R_2 and thus better T_{st} [3].

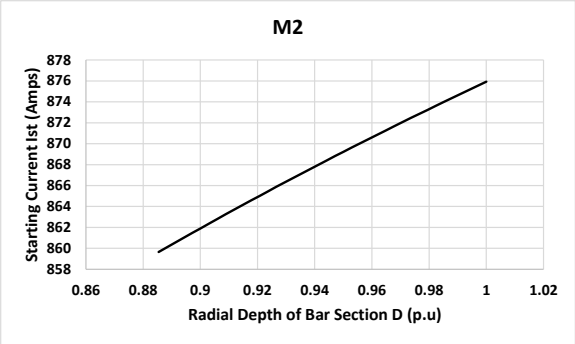

Fig 6a: Influence of change in bar radial depth on starting current (Machine M2).

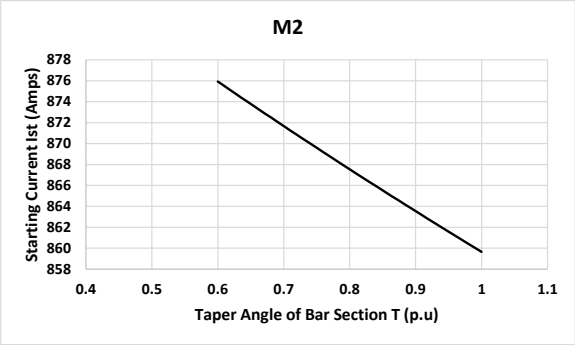

Fig 6b: Influence of change in bar taper angle on starting current (Machine M2).

A close look at Figs 6 and 7 shows that the bar radial depth (D) seems to be inversely proportional to the R_2 and tends to be increasing with I_{st}. But this doesn't appear true, because from "(1.3)" we learn that skin effect increases with D and this will likely support the rise in R_2 and thus keep I_{st} in check [17]. However, this observation may be explained by the fact that; if for instance D and T, each experience an equal percentage change, T seems more likely to impart a stronger influence on R_2 through its direct effect on the area of the bar top, than the case of trying to influence R_2 indirectly via the skin effect from bar depth.

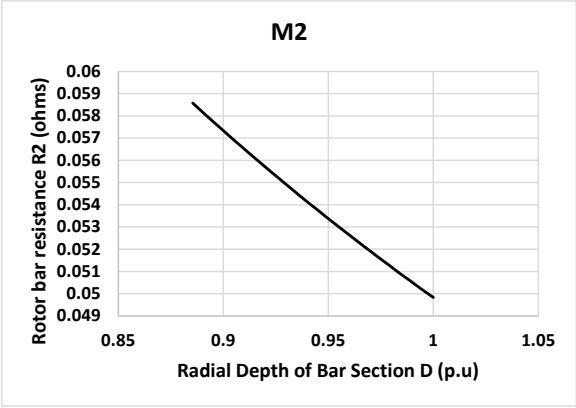

Fig 7a: Influence of change in bar radial depth on rotor resistance (Machine M2).

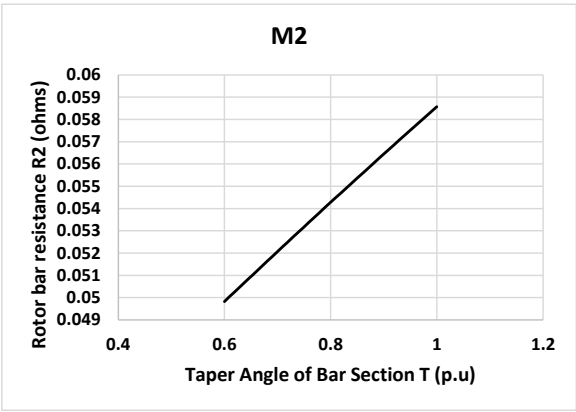

Fig 7b: Influence of change in bar taper angle on rotor resistance (Machine M2).

The effect of T on R_2 and I_{st} will likely overshadow the effect of D, and hence the figures for D appear to reflect a trend that negates theory. That perhaps explains why T seems to be inversely proportional to the I_{st} but increases with R_2; which fully enjoys the support of "(1.4)". It may therefore hold true to deduce that R_2 for this bar is largely governed by changes in T.

Further, observing Fig 8 shows that while X_2 seems to be increasing with T, it tends to be inversely proportional to D. This should be true for the case of T as explained for M1 because the narrowing effect due to a rise in T tends to discourage the saturation of the leakage flux path as well as reduce the reluctance of the cross-slot flux path (lower W); all of which tends to support the increase in X_2.

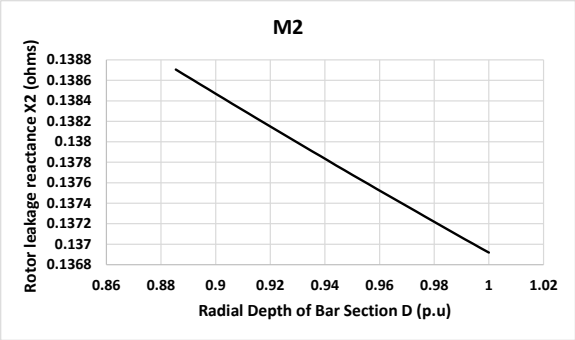

Fig 8a: Influence of change in bar radial depth on rotor leakage reactance (Machine M2).

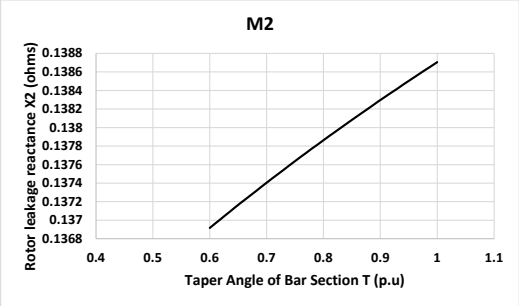

Fig 8b: Influence of change in bar taper angle on rotor leakage reactance (Machine M2).

On the other hand, the inverse relation of D with X_2 seem to have no tenable support in literature and clearly indicate that the slot leakage flux is probably not under the strong control of D. The influence of T over X_2 will again appear to dominate and cause only the T/X_2 graph of Fig 8 to stand theoretically correct. So, on both R_2 and X_2, T tends to exert a superior influence compared to D. Therefore, since R_2 and X_2 tends to depend largely on T, so does T_{st}; thereby validating only the T/T_{st} part of Fig 9.

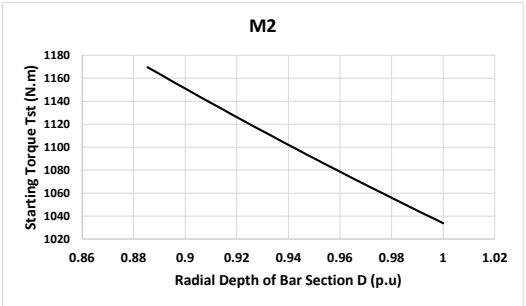

Fig 9a: Influence of change in bar radial depth on starting torque (Machine M2).

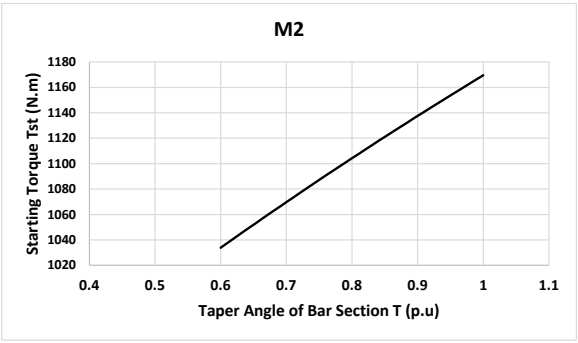

Fig 9b: Influence of change in bar taper angle on starting torque (Machine M2).

IV. TEST AND VALIDATION

It is to be tested that the cumulative influence of all investigated variables of the rotor bar on the production of starting torque, could also be largely achieved with the identified variables – W and T only. To carry out this test, the experimental machine was again used and a reference case for two other variants of the same machine was chosen. The first variant – the base case was the case in which the dimensions of all the investigated parameters of the rotor bar were increased together from the reference case, so as to influence torque. The second variant was the control case, in which only the top width W and the angle of taper T were allowed to vary from the reference case as well. The W of both variants were the same, but the T was different since D was held constant for the control case. The bar radial depth D was kept constant by simply pegging it at the value for the reference case; since W and T can always vary without varying the radial depth. All cases were simulated and the results are given in Table 3.

Table 3: Test results

	Starting Torque Tst (N.m)	Rotor bar top Width W (mm)	Rotor bar radial depth D (mm)	Angle of bar taper T (Degrees)	Rotor bar cross-sectional area A (sq.mm)	High slip R2 (ohms)	High slip X2 (ohms)	Starting current Ist (Amps)
Reference case	1211.621	10.48168	25.15602	9.2667948	185.6698	0.042764	0.132793	890.6528
Base case (W, D, T, C & A are varied)	1018.232	11.60119	27.84286	9.869465	222.594	0.035581	0.13354	895.2135
Control case (only W & T are varied)	1048.778	11.60119	25.15602	12.8149	185.6014	0.040744	0.143742	868.3571

On comparing the base and control cases as in Fig. 10 and Table 3 shows that when changes were made simultaneously to all the investigated geometric variables in the base case, a change of 15.96% (1018 to 1211 Nm) from the reference values was observed in the starting torque T_{st}; while it was 13.44% (1049 to 1211 Nm) for the control case – a difference of less than 3%.

It may be observed that while the control case seems to align with the base case up till the maximum torque, it appears to align with the reference case for the better part of low slip operation. This may be attributed to the fact that variation of W and T (as in the control and base cases) is strongly influential majorly at high slips. Since A (main controller of low slip R2) was held constant in the control case, it thus aligned with the reference as it approached synchronous speed.

CONCLUSION

The foregoing study presents to the SCIM designers and researchers, the rotor bar variables of priority as far as the starting torque is the (or one of the) objective function(s) for optimization. That is, the bar top width (to directly influence R_2) and the angle of taper (to influence X_2); for a type M1 SCIM. Also, for the rotor of a type M2 SCIM, the angle of taper is being presented to influence both R_2 and X_2, and the skin effect is to be invariably controlled by the bar radial depth. As far as design influence on starting torque is concerned, the relative importance of the angle of taper of the rotor slot/bar has been properly situated and found to be quite significant; as supported by the two machines investigated. It therefore seems unnecessary to introduce avoidable complexity to the engineer's design algorithms/programs and eventually, a more error prone final solution; by inputting all available T_{st} -influencing geometric parameters of the rotor, in the design and optimization routines, when just the angle of taper and perhaps the top width of the rotor bar, as observed, could do the job remarkably well.

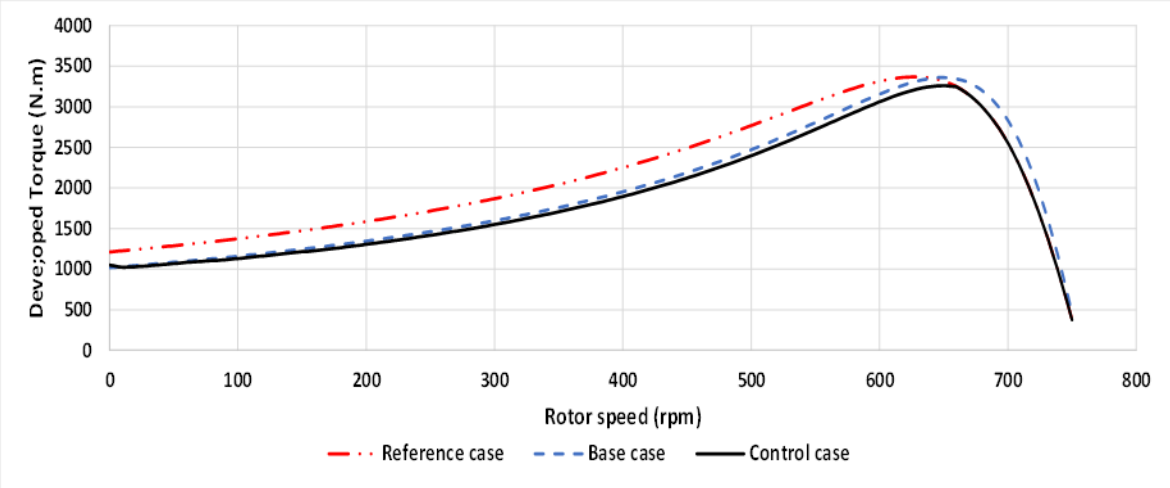

Fig 10: Test result

REFERENCES

[1] O. A. Turcanu,, T. Tudorache, and T. Fireteanu (2006). Influence of squirrel-cage bar cross-section geometry on induction motor performances. A paper presented at the International Symposium on Power Electronics, Electrical Drives, Automation and Motion.in Sicily, Italy. held at Taormina on the 23 – 26 May, 2006.

[2] M. Di Nardo, A. Marfoli, M. Degano, C. Gerada and W. Chen (2020). Rotor design optimization of squirrel cage induction motor - part II: results discussion. *IEEE*. 1 – 9. Doi: 10.1109/TEC.2020.3020263. 30 July, 2021.

[3] E. Maloma, M. Muteba and D. Nicolae (2017). Effect of Rotor bar Shape on the Performance of Three Phase Induction Motors with Broken Rotor Bars. 2017 international conference on optimization of electrical an electronic equipment (OPTIM). 364 – 369. Doi:10.1109/OPTIM.2017.7974997. 17 September, 2021.

[4] N. S. Vukosavic (2013). *Electrical Machines*. Springer New York Heidelberg Dordrecht London. ISBN: 978-1-4614-0400-2 (www.springer.com). DOI: 10.1007/978-1-4614-0400-2. Pp. 365 – 472.

[5] I. Boldea and S. A. Nasar (2010). *The Induction Machine Handbook.* Washington, D.C: CRC Press, Taylor & Francis Group. PP. 447 – 473.

[6] V. Fireteanu (2008). Squirrel-Cage Induction Motor with Intercalated Rotor Slots of Different Geometries. XIII International Symposium on Electromagnetic Fields in Mechatronics, Electrical and Electronic Engineering, September, 2007. DOI: 10.3233/978-1-58603-895-3-284.

[7] W. Purwanto, T. Sugiarto, H. Maksum, M. Martias, M. Nasir and A. Baharudin (2019). Optimal design of rotor slot geometry to reduce rotor leakage reactance and increase starting performance for high-speed spindle motors. *Advances in Electrical and Electronic Engineering.* 17 (2). 96 – 105, Doi: 10.15598/aeee.v17i2.3170. 30 July, 2021.

[8] P. L. Cochran (1989). *Polyphase Induction Motors. Analysis Design and Application*. Marcel and Dekker. NY. USA. ISBN 0-8247-8043-4. Pp. 427 – 585.

[9] M. J. Akhtar, R. K. Behera and S. K. Parida (2014). Optimized Rotor Slot Shape for Squirrel Cage Induction Motor in Electric Propulsion Application. IEEE 6th india international conference on power electronics (IICPE) 2014. 1 – 5. Dol: 0.1109/IICPE.2014.7115846. 17 September, 2021.

[10] A. G. Yetgin and M. Turan (2016). Effects of rotor slot area on squirrel cage induction motor performance. *International Journal of Innovative Science, Engineering & Technology*. 3 (11),105 – 109. Retrieved from www.ijiset.com. on 29 July 2021.

[11] S. Ho (1996) Analysis and Design of AC Induction Motors with Squirrel Cage Rotors. Doctoral Dissertations. University of New Hampshire, Durham. Retrieved from: https://scholars.unh.edu/dissertation/1909, on 22 September, 2021.

[12] B. L. Theraja and A. K. Theraja (2008). *A Textbook of Electrical Technology*. S. Chand Publishing.

[13] J. B. Gupta (2013). *Theory and Performance of Electrical Machines.* S. K. Kataria and Sons. New Delhi, India. www.skkatariaandsons.com. Part III, Pp. 359 – 439.

[14] K. De Brabanter, P. Karsmakers, F. Ojeda, C. Alzate, J. De Brabanter, K. Pelckmans, B. De Moor, J. Vandewalle and J. A. K. Suykens (2011). *LS-SVMlab Toolbox User's Guide version 1.8. ESAT-SISTA Technical Report 10-146*. http://www.esat.kuleuven.be/sista/lssvmlab/.

[15] A. Boglietti, A. Cavagnino, & M. Lazzari (2007). Geometrical Approach to Induction Motor Design. The 33rd Annual Conference of the IEEE Industrial Electronics Society (IECON). Nov., 2007, Taipei, Taiwan. 1-4244-0783-4/07/$20.00. IEEE.

[16] H. J. Lee, H. S. Im, D. Y. Um and G. S. Park (2017). A design of rotor bar for improving starting torque by analyzing rotor resistance and reactance in squirrel cage induction motor. *IEEE Transactions on Magnetics. 54 (3),* 8201404. Doi:10.1109/TMAG.2017.2764525. 30 July, 2021.

[17] T. A. Lipo (2017). *Introduction to AC Machine Design.* New Jersey: IEEE Press, John Wiley & Sons, Inc. PP. 251 – 302.

[18] H. A. Toliyat and G. B. Kliman (2004). *Handbook of Electric Motors.* Florida: Taylor & Francis Group.

[19] J. Pyrhonen, T. Jokinen and V. Hrabovcova (2014). *Design of Rotating Electrical Machines.* West Sussex: John Wiley & Sons, Ltd. PP. 293 – 388.